Investigating the thermal properties of *n*-hexacosane/graphene composite: A highly stable nanocomposite material for energy storage application

Sakshum Khanna [a,b,*], Sagar Paneliya [b], Parth Prajapati [b], Rakesh Chaudhari [b], Jay Vora [b], Hussam Jouhara [c,d,*]

[a] *Journal of Visualized Experiments, Delhi 110016, India*
[b] *School of Technology, Pandit Deendayal Energy University, Gandhinagar 382421, Gujarat, India*
[c] *Heat Pipe and Thermal Management Research Group, College of Engineering, Design and Physical Sciences, Brunel University London, UB8 3PH, UK*
[d] *Vytautas Magnus University, Studentu Str. 11, LT-53362 Akademija, Kaunas Distr., Lithuania*

ARTICLE INFO

ABSTRACT

The present work demonstrates a modified chemical synthesis route (chemical, hydrothermal methods, and sonication) for fabricating *n*-hexacosane-impregnated graphene nanosheets (GrPCM) nanocomposite, exhibiting enhanced thermal stability in energy storage. The exfoliation of the graphene sheet during the hydrothermal and sonication process increases the surface area that can absorb *n*-hexacosane, improving the impregnation and interaction between them. Scanning electron microscopy (SEM), X-ray diffraction (XRD), and Raman spectroscopy were used to examine the morphological and structural characteristics of the GrPCM nanocomposite. The findings demonstrate the loading of *n*-hexacoreferesane PCM materials into porous nanosheet structures without any chemical reactions. Thermo-gravimetric analysis (TGA), differential scanning calorimetry (DSC), and infrared thermography (IR) were used to measure the latent heat, mass loss, thermal conductivity, and stability of as-synthesized GrPCM nanocomposites. The melting and solidification of GrPCM nanocomposite were observed at 57.11 °C with a latent heat of 154.61 J/g and 49.28 °C with a latent heat of 147.58 J/g, respectively. The GrPCM nanocomposites showed a thermal conductivity of 12.63 W/m K, which is enhanced compared to that of pure PCM materials of around 0.26 W/m K. Thermal performance measurements using infrared thermography revealed a significant increase in the nanocomposite's thermal conductivity over *n*-hexacosane, which was attributed to the reduced graphene nanosheet. Further, to study the heat transfer between fluid and different nanocomposites, the GrPCM nanocomposites were investigated inside a thermal storage tank. The experimental results were found in agreement with the COMSOL simulation and confirms GrPCM3 to be an excellent composite material for efficient heat transfer processes.

Introduction

Using renewable energy sources and improving energy efficiency techniques has become increasingly important in today's world due to continuously rising greenhouse gas emissions and fossil fuel prices [1,2]. In addition to being essential for the efficient use of renewable energy sources, thermal energy storage systems also contribute to improving a wide range of applications and processes' energy efficiency. Thermal energy storage has been used to store the heat from solar energy, absorbed during the day and released at night [3]. Phase change materials (PCMs) are the types of materials that absorb or emit a considerable amount of heat throughout the phase change at a particular temperature [4]. The ability of PCMs to absorb or release heat during their phase-changing process makes them highly sought-after among thermal energy storage (TES) materials [5–7]. *N*-hexacosane (Paraffin wax), an organic phase change material, is one of the most extensively used materials for thermal energy storage due to its high energy storage capability, chemical inertness, low cost, low vapor pressure, and ability to exhibit a wide transition temperature range [8,9]. However, the major drawbacks of such PCMs (like *n*-octadecane, paraffin wax, *n*-nonadecane, and other alkanes) are high volumetric expansion, low thermal conductivity, and leakage during the phase transition, which
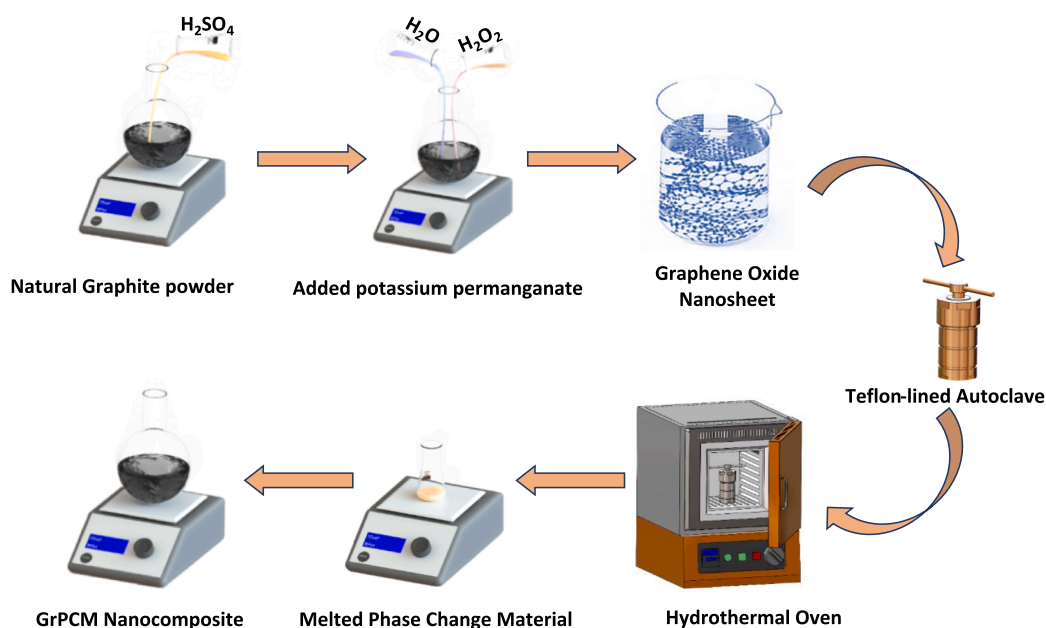
Fig. 1. Illustration of the synthesis process for synthesizing *n*-hexacosane-impregnated graphene nanosheet (GrPCM) nanocomposite.

directly limit the overall thermal performance of the energy storage system. To overcome the aforementioned drawbacks, several studies have used polymer blending [10,11], micro/nano-encapsulation [12,13], or encapsulation with porous materials to solve the leakage problem.

Additionally, numerous studies have added high thermal conductivity additives to organic PCMs to increase their thermal conductivity for better thermal performance [14–16]. A review by Khodadadi et al. (2013) covers a wide range of topics regarding many of these recent initiatives to improve the thermal conductivity of PCM. These studies suggest that encapsulation and nanoparticle mixing should be appropriately done to increase the PCM's thermal conductivity significantly.

Carbon nanomaterials like reduced graphene oxide (RGO), carbon dots (CD), exfoliated graphite (EG), graphene (Gr), and carbon nanotubes (CNT) have been used as thermal conductive additives because they offer better thermal conductivity with good stability [17].

In 2011, Cui et al. [18] experimentally explored the thermal behavior of phase change material using carbon nanostructure additives. Similarly, in 2013, Li et al. [19] experimentally investigated the enhancement of heat transfer for thermal energy storage applications using a stearic acid nanocomposite with multi-walled carbon nanotubes. Additionally, different nanocomposites use various binding strategies and composite material ratios to take advantage of the PCM contained within the graphitic nanostructure [20–25]. D. Zhou et al. [26] investigated myristic acid loaded expanded graphite nanocomposite material, where the phase change material liquid was absorbed between the expanded graphite nanosheet. The results indicated an enhancement in the stability and thermal conductivity of the phase change material.

By proving that graphene is present in organic phase change materials, Kalaitzidou et al. [27] showed in 2007 that the presence of graphene unquestionably increases the base material's thermal conductivity. According to Fan et al. [28], adding 3 % more graphene to a paraffin wax resulted in a thermal conductivity twice as high as for the base material. Furthermore, Tao et al.'s [29] thermal characterization of graphene-reinforced paraffin wax in 2015 showed a maximum improvement in thermal conductivity of almost 28 % for 2.5 wt% graphene. Recently, M. Amin et al. [30] investigated the thermophysical properties of beeswax/graphene phase change material for building applications. The finding revealed that the latent heat and heat capacity of beeswax/graphene was increased by 22.5 % and 12 %, respectively.

The thermal conductivity of beeswax/graphene obtained was 2.8 W/m K, which was highly enhanced compared to pure phase change material.

The aforementioned results showed that the nanocomposite's thermal conductivity had substantially increased as the carbon content increased. But there is still much room for improvement regarding the stable encapsulating material with PCM, thermal performance, and encapsulation mechanism. It is important to continue researching the thermophysical properties of the *n*-hexacosane (PCM)/graphene nanocomposite (GrPCM), which could regulate the surplus thermal energy in various applications.

Graphene (Gr) serves as the porous supporting material, and *n*-hexacosane (PCM) is the active material in the nanocomposite we present here, which is a stable thermal energy storage material. The synthesized route offers high PCM impregnation in porous graphene materials and balances ratios of the latent heat to the thermal conductivity of the PCM. The physical, chemical, and structural characteristics of as-synthesized GrPCM were examined using transmission electron microscopy (TEM), scanning electron microscopy (SEM), Raman, and X-ray diffraction spectroscopy. On the other hand, thermogravimetric analysis (TGA), differential scanning calorimetry (DSC), and 2-wire methods were used to investigate the phase change temperature, thermal decomposition temperature, latent heat, and thermal conductivity. Supercapacitors, rechargeable batteries, electric vehicles, and energy storage devices are examples of high-temperature environments where the GrPCM nanocomposites may be applied for better performance.

Experimental methodology

Reagents

N-hexacosane or paraffinic hydrocarbons are straight-chain saturated organic compounds with the composition C_nH_{2n+2}. *N*-hexacosane is a frequently used phase change material due to its chemical stability, availability, and durability in cycling. Phase change material (*n*-hexacosane), Natural flake graphite (NG) (99 wt%) with flake size of 150 ~ 200 nm, sodium nitrate, sulphuric acid (98 wt%), phase change material (*n*-hexacosane), and hydrogen peroxide (30 wt%) were procured from Sigma Aldrich, India and were used without any modification.

Table 1
Packing density of various GrPCM composites.

S. No.	Material	Carbon Quality (%)	PCM (%)	Packing Density (kg/m^3)
1.	n-hexacosane	-	100	-
2.	GrPCM1	5	95	633.22
3.	GrPCM2	10	90	687.37
4.	GrPCM3	15	85	746.58

Synthesis of graphene oxide

A modified Hummer technique was used to synthesize graphene oxide. In a nutshell, 20 mL of concentrated sulphuric acid was combined with 1:1 ratios of sodium nitrate and graphite flakes, and the mixture was then placed in an ice bath for five hours. The solution was then slowly stirred for 10 h while 2.0 g of KMnO$_4$ was added. Then 40 mL of De-ionized water was added dropwise, the solution was heated at 90 °C for 45 min, and subsequently a mixture of water and H$_2$O$_2$ (80:5 mL) was added. Later, the solution was centrifuged at 7000 rpm and washed multiple times with DI water (pH = 7) [31]. For further use, the concentration of the solution obtained was eventually adjusted to 0.5 mg/mL (Gr1), 1 mg/mL (Gr2), and 2 mg/mL (Gr3).

Synthesis of graphene

The liquid dispersion was shifted to a 30 mL-Teflon-lined autoclave and heated in an oven at 200 °C for 2 hrs. The obtained product appeared in black and was named graphene (Gr). The resultant product showed high dispersion with no aggregates. In preparation for future nanocomposite samples, the suspensions were vacuum-filtered and allowed to dry at room temperature.

Synthesis of Graphene/n-hexacosane (GrPCM) nanocomposite

The filtered graphene solution was sonicated for 45 min to exfoliate the graphene nanosheets before adding melted PCM (10 g) and then stirred for 60 min for improved impregnation of PCM between the graphene nanosheet. The final product was filtered and dried overnight after being washed a few times with DI water. Further, the overnight sample was placed in a muffle furnace for 2hrs at 50 °C to obtain GrPCM nanocomposite, as shown in Fig. 1.

Different samples were created using the above chemical procedures and labeled GrPCM1, GrPCM2, and GrPCM3, as shown in Fig. 1, depending on the graphene content (5 wt%, 10 wt%, and 15 wt%) with *n*-hexacosane. Furthermore, using a hydraulic press with a pressure of 50 kg/cm^2 and a diameter and height of 1 cm, various GrPCM pellets were shaped into cylindrical blocks. The packing densities were determined by converting formed masses of cylindrical blocks to volumes, as shown in Table 1.

Instrumentation

Structural and morphological instrument

The chemical and structural characteristics of as-synthesized GrPCM samples were investigated using Fourier Transform Infrared Spectroscopy (FTIR, Malvern), X-ray Diffraction (Panalytical, X'PertPRO, λ = 1.54; Powder mode with 2θ ranging from 10° to 70°), and Raman Spectroscopy (Renishaw in via Raman microscope, laser of wavelength 532 nm). In addition, the surface analysis of the sample was recorded using a Transmission Electron Microscope (TEM) (JEOL 2100) operating at 200 keV with a point-to-point resolution of 0.19 nm and a Field Emission-Scanning Electron Microscope (FESEM) (Zeiss Ultra 55) operating at 5 keV.

Thermal analysis

A differential scanning calorimeter (DSC) (PerkinElmer DSC 8000) having temperature range till 750 °C was used to measure the phase transition temperature and latent heat of the GrPCM nanocomposite. The sample was weighed and sealed in an aluminum pan prior to measurement. It was then measured with accuracy and precision of ± 0.04 °C and ± 0.007 °C using a heating rate of 3 °C/min under a constant stream of argon at a flow rate of 10 mL/min. The PCM mass for each test was ∼ 4–4.35 mg. The theoretical latent heat was determined using the equation below to ascertain the experimental results' error.

$$\Delta H_{GrPCM} = (1 - W_{Gr}\%) \times \Delta H_{PCM} \tag{1}$$

The PerkinElmer thermogravimetric analyzer (TGA 4000) with a heating rate of 5 °C/min from 27 °C to 600 °C was used to measure weight loss or mass fraction. For each PCM nanocomposite, the average result of the tests on five replicates was reported.

The thermal conductivity of numerous GrPCM samples was analyzed using the transient hot-wire technique, see Figure S1 (please refer to supplementary information) from Paneliya, Khanna, et al. [32]. The thermal diffusivity of the nanocomposite samples was calculated indirectly from the thermal conductivity of GrPCM [33].

A *t*-history method was used to investigate the heat storage and release properties of the PCMs. The equipment comprised K-type thermocouple probes intercalated into the middle of the individual sample and sealed with rubber stoppers. Individual test tubes were added to the water bath and heated to 70 °C. Once the temperature stabilized at 70 °C, the test tubes were shifted to another water bath at 25 °C room temperature. A data acquisition instrument with a ± 0.1 °C accuracy was used to measure the temperature variation of each nanocomposite over time and log it once every-two seconds.

Thermal storage tank

A heat storage tank was fabricated to investigate the performance of as-synthesized GrPCM during thermal cycling. The entire setup of storage tank having diameter of 154 mm consists of three sections, the first and third section of the tank was used as the inlet and outlet for the fluid, whereas the middle section was used for heat storage between the PCM and fluid. The middle section was fabricated with five cylindrical copper tubes each having a diameter of 10 mm for effective heat transfer. The thermal storage setup was completely insulated to obtained efficient heat storage and to reduce the heat loss in the surrounding.

The parameters which have been investigated to estimate the performance of the system during the thermal cycling are temperature and time. The amount of time it takes to keep the water at the same temperature is based on the amount of heat exchanged with the GrPCM and the rise in the temperature of the PCM temperature. The energy is stored in the phase change material system as both latent and sensible heat. An effective heat storage system consisting of phase change materials requires minimal charging (melting) time and confines the phase change (S-L) within graphene nanosheets. During the process, the latent heat of fusion (HF) (J/kg), latent heat (HLH), sensible heat (HS), and overall heat stored (ET) in the phase change material storage system can be obtained by the following equations:

$$E_s = mC_p(T - T_i) \tag{2}$$

$$E_{LH} = mH_f\theta \tag{3}$$

$$E_T = mC_p(T - T_i) + mH_f\theta = E_s + E_{LH} \tag{4}$$

COMSOL software based simulation.

Heat transfer is one of the engineering phenomena that can be simulated by COMSOL Multiphysics in a single environment. COMSOL simulation provides a systematic approach and understanding of the
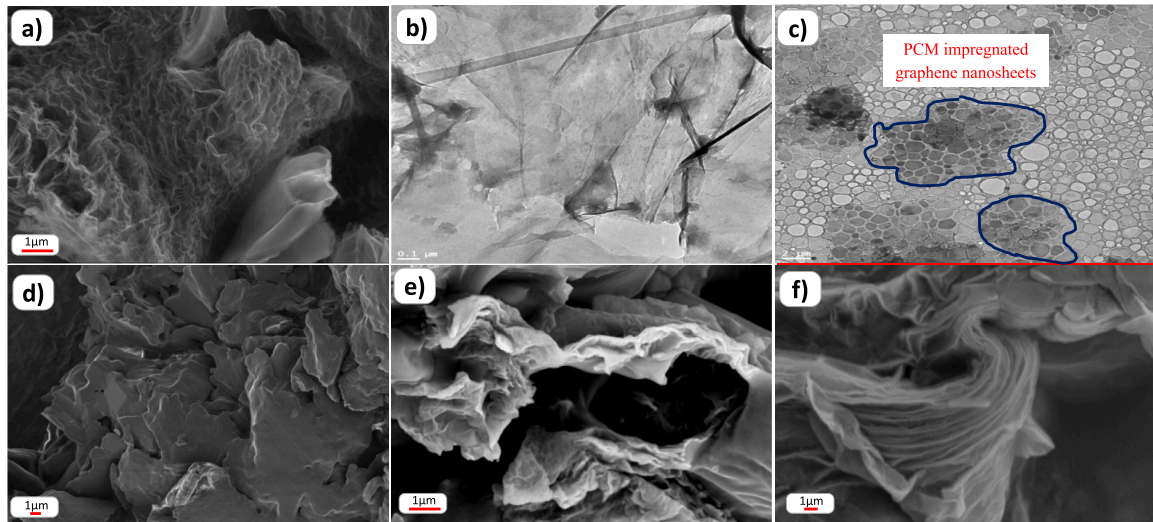
Fig. 2. (a) FESEM, (b) TEM images of graphene nanosheet, (c) TEM micrograph of GrPCM and FESEM of various carbonaceous content, (d) 5 wt% (e) 10 wt% and (f) 15 wt%.
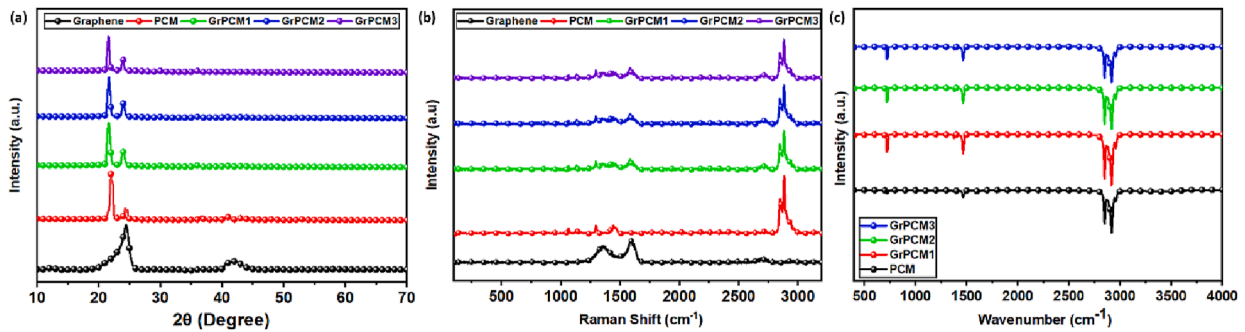

Fig. 3. (a-b) XRD Raman profile and (c) FT-IR spectra of graphene, phase change material, and GrPCM nanocomposites.

heat transfer process inside the storage tank and melting/solidification of the phase change material with respect to the change in the carbon concentration. A temperature of 70 °C was provided as the input at the inlet source, and simulations for constant heat flux conditions were carried out. When heat flux is applied, melting begins, and phase change material absorbs the energy and stores it as latent energy, which can be used later. The equations for the conservation of energy, mass, and momentum were used for the simulation, as follows: [6,32,33].

Mass Conservation:

$$\frac{\partial \rho}{\partial t} + \nabla \bullet \rho \overrightarrow{V} = 0 \qquad (5)$$

Momentum Conservation:

$$\rho \frac{\partial \overrightarrow{V}}{\partial t} + \rho \left(\overrightarrow{V} \bullet \nabla \right) \overrightarrow{V} = -\nabla P + \mu_f \left(\nabla^2 \overrightarrow{V} \right) - \overrightarrow{g}(\rho \alpha_p)(T - T_m) \qquad (6)$$

Energy Conservation:

$$\rho C_p \frac{\partial T}{\partial t} + \nabla \rho C_p \overrightarrow{V} T + \nabla \bullet q = Q + Q_p + Q_{vd} \qquad (7)$$

where,

μ_f = dynamic viscosity of PCM,

T_m = Melting temperature (K).

α_p = Coefficient of thermal expansion in a fluid (1/K).

τ = Viscous stress tensor.

Q = Heat source(W/m^3).

Q_p = Point heat source (W/m^3).

Q_{Vd} = Viscous dissipation (W/m^3).

Cp = Specific heat capacity at constant pressure (J/(kg·K))

$\overrightarrow{V}$ = Velocity Vector (m/s)

Result and discussions

Surface morphological analysis

Fig. 2(a) displays FESEM images of hydrothermally produced graphene nanosheets. Fig. 2 (b) depicts the thin intercalated graphite layers that were analyzed using TEM imaging. A large sheet of micrometer-sized graphene has been observed on top of the grid, exhibiting transparent and rippled silk wave appearances. According to earlier reports in the literature, graphene's inherent characteristics include folds and wrinkles because bending makes the 2D membrane structure thermodynamically stable [34]. Additionally, a portion of the graphene sheet has a relatively flat morphology and low contrast, which indicates a thin layer thickness. A significantly 2D porous nanostructure with a sheet length of 300–500 nm was observed, which also provides mechanical strength for the impregnation of phase change materials, as shown in Fig. 2(c) [35].

Additionally, numerous nanoscale pore structures in the synthesized graphene were found using Brunauer-Emmett-Teller (BET) analysis. N$_2$ desorption/adsorption isotherms of graphite and graphene are shown in Figure S2 (please refer to supplementary information). Both of the carbon materials showed Type III isotherms, which suggests that the adsorbent materials contain a lot of pores. In contrast to pristine graphite, graphene had significantly higher BET surface area and total
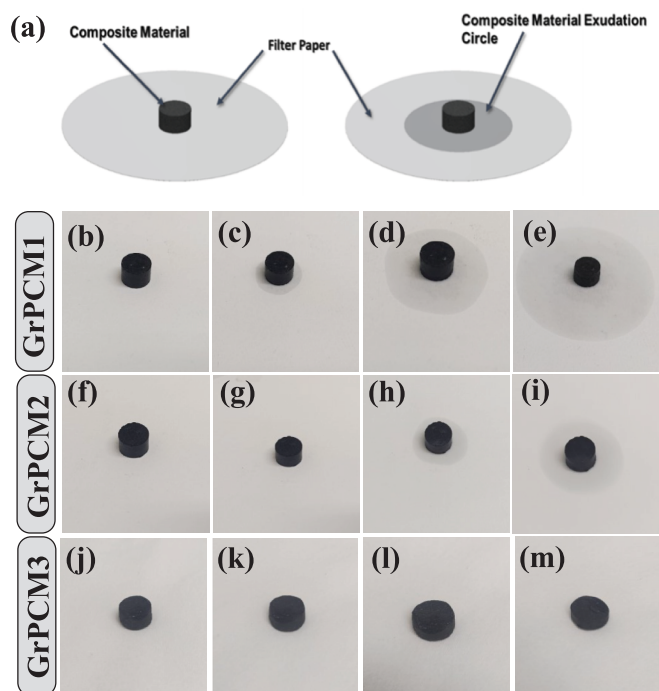
Fig. 4. (a) Schematic of Exudation-circle test diagram and various GrPCM samples (b-e) 5 wt%, (f-i) 10 wt% and (j-m) 15 wt%.

Table 2
Leakage test assessment of GrPCM composite.

Level of exudation	Avg. Circle diameter (exudation)	Leakage (%)	Range of Ψ (%)	Stability
GrPCM1	15.85	58.5	Ψ > 50	Very unstable
GrPCM2	12.28	22.8	15 < Ψ < 30	Stable
GrPCM3	10.58	5.8	Ψ < 10	Extremely Stable

pore volume; for example, the surface areas of graphene were ~ 39 m^2/g, whereas those of pristine graphite were ~ 3.3 m^2/g. As a result, this structure contributes to a large volume and high surface area and can have a high adsorption capacity. The morphology of various GrPCM nanocomposites before melting and solidifying cycles is shown in Fig. 2 (d-f). The porous structure of the graphene nanosheet did not change significantly at lower carbon contents. The impregnation of phase change material reduces the overall pores in the 2D structure and substantially depends on the graphene mass. Excess formation of n-hexacosane materials was observed on the surface of the nanosheets, which indicates the maximum ability of graphene was reached to absorb them [32]. This suggests that the graphene nanosheets' capillary force was insufficient, causing PCM to agglomerate outside porous nanostructures, as shown in Fig. 2(d-e) [36]. Additionally, on increasing the carbon wt. % to 15 %, high PCM impregnation was seen, filling every microstructure of the carbonaceous material. The remaining 2D nanostructures of graphene contribute to enhancing the electrical and thermal conductivity of the synthesized GrPCM nanocomposites (Fig. 2(f)).

Structural and chemical analysis

Fig. 3(a) illustrates the results of an X-ray diffraction spectroscopy analysis of the crystallinity of PCM (n-hexacosane), graphene, and the GrPCM nanocomposites. The PCM characteristic peaks were found at

23.62° and 21.13°, corresponding to the (2 0 0) and (1 1 0) crystal planes of the compound (JCPDS No. 40–1995). Moreover, no additional peaks were identified in GrPCM nanocomposite other than characteristic peaks of graphene and PCM at and 21.13°, 23.62°, and 26.68° indicating unaltered PCM even after the synthesis process [33]. The result confirms that the physical mixing and compression method has been used in synthesizing different nanocomposites. Also, the peak intensity in GrPCMs is lower than that of the carbonaceous materials, suggesting that when the molten n-hexacosane is impregnated between the graphene nanosheets, the graphite crystal structure degrades. This deterioration in the graphitic crystal structure has an impact on the GrPCM's thermal conductivity [37].

The Raman spectra of graphene, PCM, and GrPCM nanocomposite are shown in Fig. 3(b). The characteristic peaks of PCM were recorded at 1057 cm^{-1}, 1152 cm^{-1}, 1297 cm^{-1}, and 1461 cm^{-1} and were attributed to methylene (CH$_2$) and methyl group (CH$_3$) deformation and carbon–carbon stretching [13]. Graphene and graphite's primary Raman peaks, designated 2D, G, and D bands, were observed at 2710 cm^{-1}, 1585 cm^{-1}, and 1354 cm^{-1}, respectively. The presence of 2D bands is the distinguishing characteristic of natural graphite and graphene, as shown in Figure S3 (supplementary information). A red shift of the 2D band for graphene was seen compared to natural graphite. The Raman spectra exhibit some defects, as indicated by the D band and a 2D band with an ID/IG ratio of < 1, indicating lower defects and improved aromatic structure [31,42]. The chemical exfoliation that takes place during the hydrothermal process may be the cause of these flaws [38]. As a result, the method enables the production of high-quality graphene on a large scale using low-cost methods.

The Fourier transform infrared (FT-IR) spectroscopy results of phase change material and GrPCM nanocomposites are demonstrated in Fig. 3 (c). The FT-IR spectra in pure n-hexacosane (PCM) display vibrational peaks at 720 cm^{-1}, 1380 cm^{-1}, and 1466 cm^{-1} attributed to CH$_2$ (methylene) and C—H bonds. Additionally, the stretching vibration maxima of the C—H bond's symmetrical and asymmetrical forms were found to be at 2849 cm^{-1} and 2914 cm^{-1}, respectively [31–33]. The initial peaks in the spectrum did not change after adding n-hexacosane to the 2D nanosheet chemically, and no new peaks were seen for varying carbon contents. The lack of new peaks in the FTIR and Raman spectra confirms that the loading is by physical attachment and excludes any possible chemical interaction between the components.

Absorption ratio in GrPCM nanocomposites

In general, as the mass of the phase change material in nanocomposites increases the latent heat absorption increases, thus making it a better material for TES systems. But the major issue with increasing the phase change materials is the leakage problem. In the case of GrPCM nanocomposites, n-hexacosane (PCM) impregnates the graphene nanosheets, which act as a supporting matrix to the material. The phase change material (PCM) changes from a solid to a molten state during the melting process, but the leakage of the PCM is constrained by physical adhesion and capillary forces between the primary PCM material and the matrix (graphene). Beyond the graphene's maximum capacity for absorption, extra phase change material tries to bind to the surface of the carbon nanomaterial and exude during the phase-transition process. The difference in the mass fraction of carbon (graphene nanosheets) influences the temperature at which phase transitions occur and enhances matrix absorption. Therefore, the mass rate of phase change material in PCM nanocomposites was verified using the diffusion-exudation circle method [26]. Fig. 4 illustrates the process and the test method diagram [29]. In order to make GrPCM nanocomposite pellets with a diameter of 1 cm, PCM with various graphene contents were processed. Initially, the sample was kept over the filter-paper (at 70 °C) and removed after 20 min. Fig. 4 illustrates the degree of n-hexacosane leakage observed in various nanocomposites outside the unit test area. According to the amount of leakage, they can be classified as unstable stable, or extreme
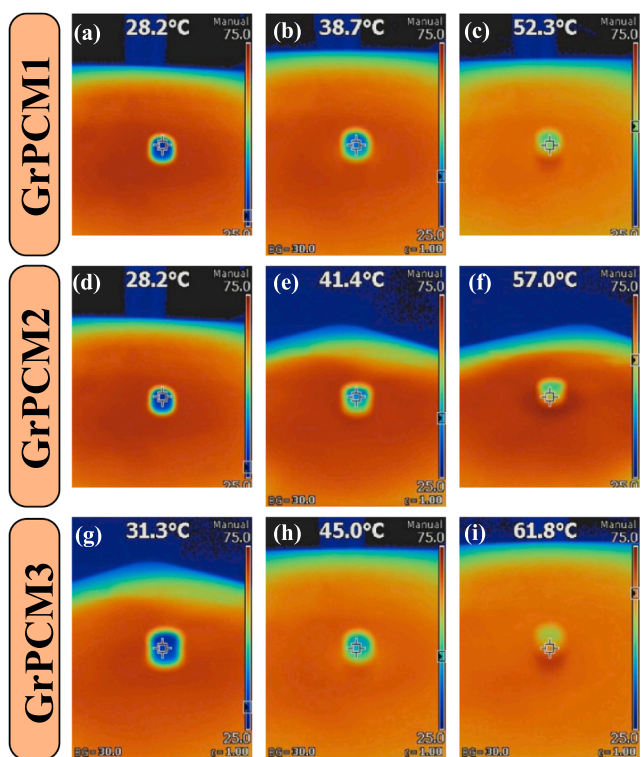
Fig. 5. Infrared imaging of various GrPCM nanocomposites.

determined by the diffusion-exudation method. Infrared imaging was done for various GrPCM nanocomposites to investigate the temperature changes related to graphene content. Graphene nanosheets loaded with PCM composites and pure PCM surface temperature distributions were measured, and the average surface temperatures were computed, as shown in Fig. 5. The pellets with lower graphene content leaked, whereas samples with higher graphene content, such as the GrPCM3 sample (15 wt%), showed no exudation. Hence, the GrPCM3 was found to be a stable nanocomposite compared to other samples. The findings showed that the GrPCM composite effectively transferred heat over a shorter period of time due to the increase in carbon content.

Thermal analysis of GrPCM composite

Using a differential scanning calorimeter (DSC), the phase transition temperatures and latent heats of *n*-hexacosane, GrPCM1, GrPCM2, and GrPCM3 were examined. The melting and solidifying DSC curves of GrPCM1, GrPCM2, and GrPCM3 composites of PCM, which represent the phase transition temperatures of PCM, are shown in Fig. 6(a-b). The findings reveal two-phase transition peaks at a lower and higher temperature indicating a solid–solid (S—S) and solid–liquid (S-L) phase transition with small and significant heat flow, respectively. These phase-change transitions between solids and liquids are still close to those of PCM (*n*-hexacosane), which occurred between 49.28 °C and 57.11 °C. The S—S phase transformation converts ordered to disordered phases during the melting stage [39]. Additionally, it was found that the peak and onset temperatures of GrPCM nanocomposites during the solidifying process were marginally lower than those of PCM, indicating a smaller degree of super-cooling in the GrPCM nanocomposites compared to PCM [40].

Furthermore, the aforementioned phase transition process was used to calculate the latent heat of the phase change material and GrPCM nanocomposites. The melting and cooling temperatures of *n*-hexacosane, GrPCM1, GrPCM2, and GrPCM3, as well as their latent heats (experimental and theoretical), are shown in Tables 3 and 4. The findings show that, in comparison to pure *n*-hexacosane, adding more
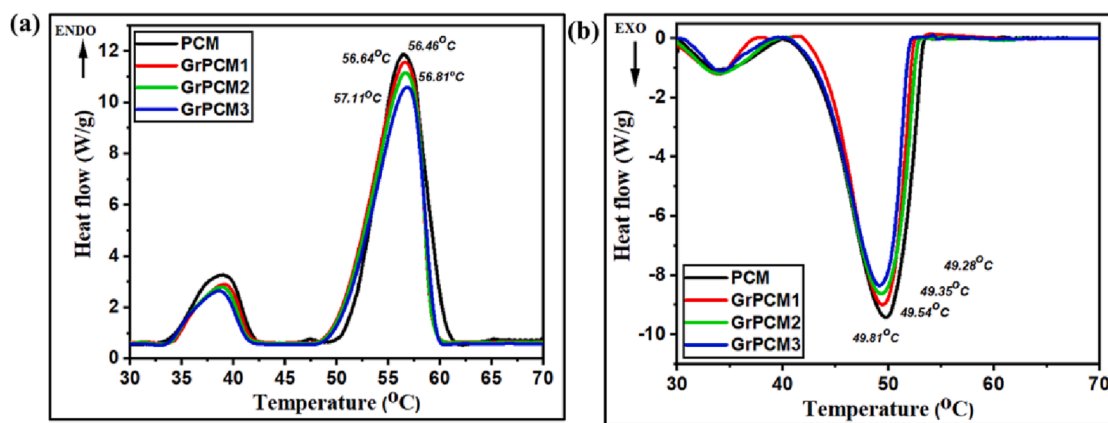
stable, as shown in Figure S4 (please refer to supplementary information).

The level of exudation and corresponding stability of samples were determined by approximating the exuded percentage (Ψ) and comparing it to the known range of standardization [32]. Table 2 lists the stability of various GrPCM nanocomposites with various carbon (Gr) contents as

Fig. 6. (a) Melting and (b) solidifying differential scanning calorimetry curves of the PCM and different GrPCM nanocomposite.

Table 3
Latent heat for various GrPCM nanocomposites before and after thermal cycles during the melting phase.

Samples	Phase Transition Temperature (°C)	1st cycle (KJ/Kg)	1st Theoretical valve of latent heat (KJ/Kg)	100th Cycle (KJ/Kg)	Phase Transition Temperature after 100th Cycle (°C)	Relative Error
PCM	56.46	185.76	-	179.04	56.32	-
GrPCM1	56.64	169.95	176.47	165.06	56.47	3.69%
GrPCM2	56.81	162.40	167.18	159.29	56.53	2.86%
GrPCM3	57.11	154.61	157.90	152.06	56.98	2.08%

Table 4

Latent heat for various GrPCM nanocomposites before and after thermal cycles during the solidification phase.

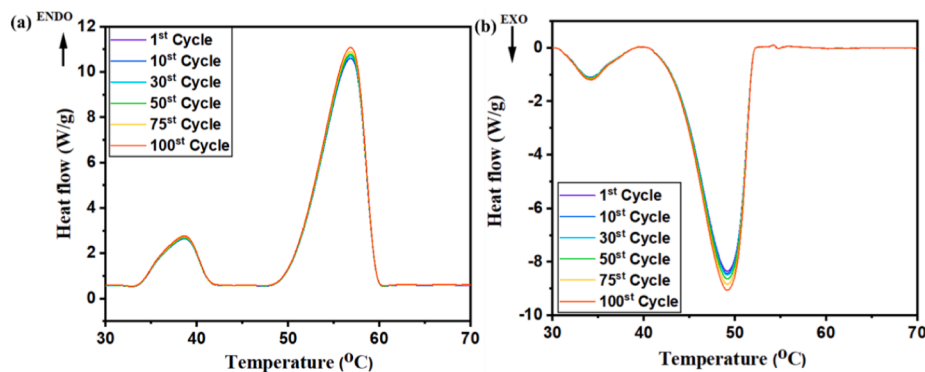| Samples	Phase Transition Temperature (°C)	1st cycle (KJ/Kg)	1st Theoretical valve of latent heat (KJ/Kg)	100th Cycle (KJ/Kg)	Phase Transition Temperature After 100th Cycle (°C)	Relative Error
PCM	49.81	179.38	-	174.79	49.41	-
GrPCM1	49.54	165.51	170.41	153.84	49.19	2.87%
GrPCM2	49.35	154.26	161.44	151.26	49.05	4.44%
GrPCM3	48.28	147.58	152.47	145.11	49.08	3.21%

Fig. 7. Thermal cycling performance of GrPCM3 nanocomposite under 100 melting and solidification cycles.
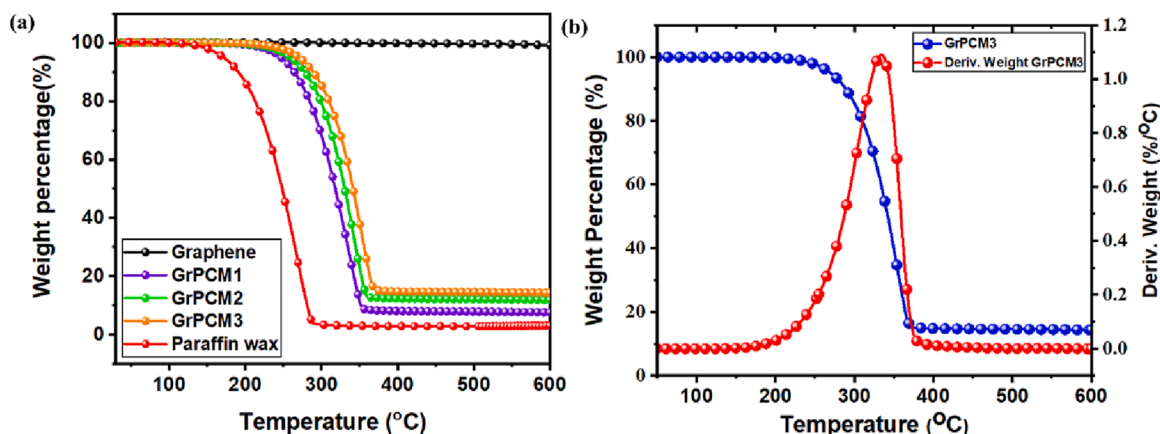

Fig. 8. (a-b) TGA analysis of various GrPCM nanocomposites.
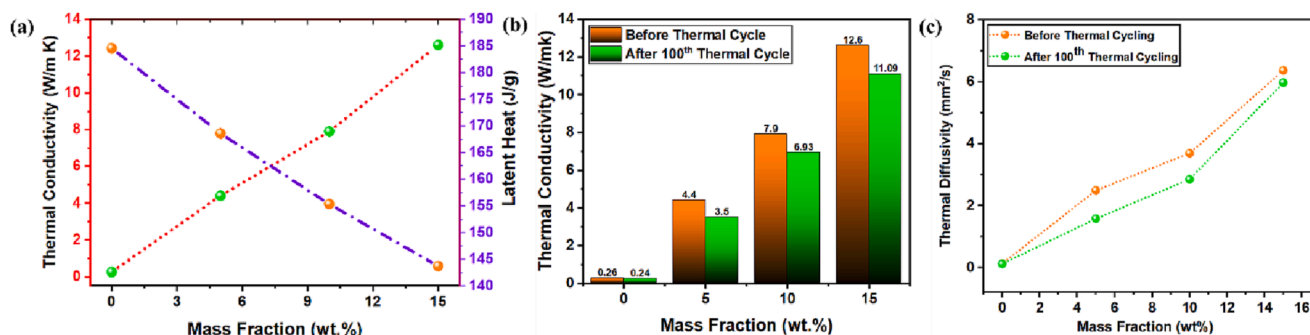

Fig. 9. (a) Relationship between Thermal Conductivity and latent heat, (b-c) Thermal conductivity and diffusivity of GrPCM nanocomposite before and after thermal cycling.

graphene reduces the heat storage capacity. This effect can be tuned by changing the carbonaceous content. The main disadvantage of lower graphene content (5 wt% and 10 wt%) is the phase change material leakage issue, which eventually lowers the nanocomposites' overall thermal conductivity and stability. Further, GrPCM3 showed a steady and promising energy storage material at higher carbonaceous content

Table 5
Enhancement of the PCM thermal conductivity by adding graphene nanosheet.

Phase change material	Gr content (wt. %)	Thermal conductivity k (W/m K)		References
		Pure PCM	Composite PCM	
Beeswax	0.05, 0.1, 0.15 0.2, 0.25, 0.3	0.25	1.15, 1.5, 1.6, 2.15, 2.25, 2.75	M. Amin et al. [47]
Stearic acid	1, 5, 10 %	0.26	0.90, 1.05, 1.12	C. Li et al. [48]
Paraffin wax (IGI-1260)	1, 5, 20	0.25	8, 15, 45	P. Goli [49]
Paraffin wax	1.5, 2	0.25	0.48, 0.54	K. Kumar et al. [43]
Octadecanoic acid	5, 9	0.15	0.32, 0.20	M. Qian et al. [50]
Paraffin wax	1, 2, 3	0.25	0.17, 0.21, 0.303	MA. Ali et al. [46]
Melamine foam /paraffin wax	0.01, 0.05, 0.1	0.28	0.25, 0.31, 0.33	W. Cui [51]
Paraffin Wax	0.1, 0.2, 0.3, 0.4, 0.5	0.26	0.33, 0.37, 0.39, 0.45, 0.45	M. Joesph [52]
n-Hexacosane	*5, 10, 15*	*0.26*	*4.43, 7.92, 12.63*	*Present Work*

with the desired heat capacity and high thermal stability. The long-term performance of any material in heat storage systems is significantly influenced by its thermal stability. Fig. 7(a-b) depicts the GrPCM3 nanocomposite material's DSC stability profile before and after a thermal cycle, demonstrating that GrPCM is a highly stable material even after 100 thermal cycles. The phase transition temperatures of GrPCM3 nanocomposites after 100 thermal cycles changed by 0.13–0.2 °C, and the phase-change latent heat changed by 2.05–3.25 %, as shown in

Tables 3 and 4, respectively. These findings suggest that when compared to pure *n*-hexacosane, GrPCM nanocomposites have good thermal-cycle reliability.

The thermal stability curves of the chemically made GrPCM nanocomposites, as determined by thermal gravimetric analysis (TGA) for thermal melting/cooling cycles, are shown in Fig. 8(a-b). All the PCMs nanocomposite weight fraction loss TGA curves were nearly identical and showed a degradation process. The thermal stability of GrPCM was examined within 190 °C-250 °C temperature ranges because pure PCM's flashpoint and boiling point (*n*-hexacosane) were approximately 360 °C. The hydrothermally produced graphene samples exhibited slight dehydration at temperatures as high as 590 °C, resulting in a weight loss of about 1.5 %. Fig. 8(a) displays the temperature at which different GrPCM nanocomposites degrade thermally when not subjected to thermal cycling. The nanocomposites tend to evaporate at about 175 °C-185 °C and entirely decay at 375 °C. Peak temperatures for the thermal decomposition of GrPCM nanocomposites were 353.66 °C, 360.16 °C, and 367.62 °C. However, graphene nanosheets are still present in the nanocomposite after complete thermal decomposition as waste. The outcome can be attributed to the catastrophe of capillary action by the graphene nanosheet in the nanocomposites during melting and solidification cycling and the exudation of *n*-hexacosane.

Thermal conductivity and diffusivity measurements of GrPCM nanocomposites

In comparison to *n*-hexacosane, the graphene nanosheets exhibited better capillary action to PCM and enhanced thermal conductivity [17,41]. The addition of graphene to the GrPCM nanocomposite is largely responsible for the nanocomposite's improved thermal conductivity. The thermal conductivities of the GrPCM nanocomposites, as measured prior to and after 100 melting and solidification cycles, are
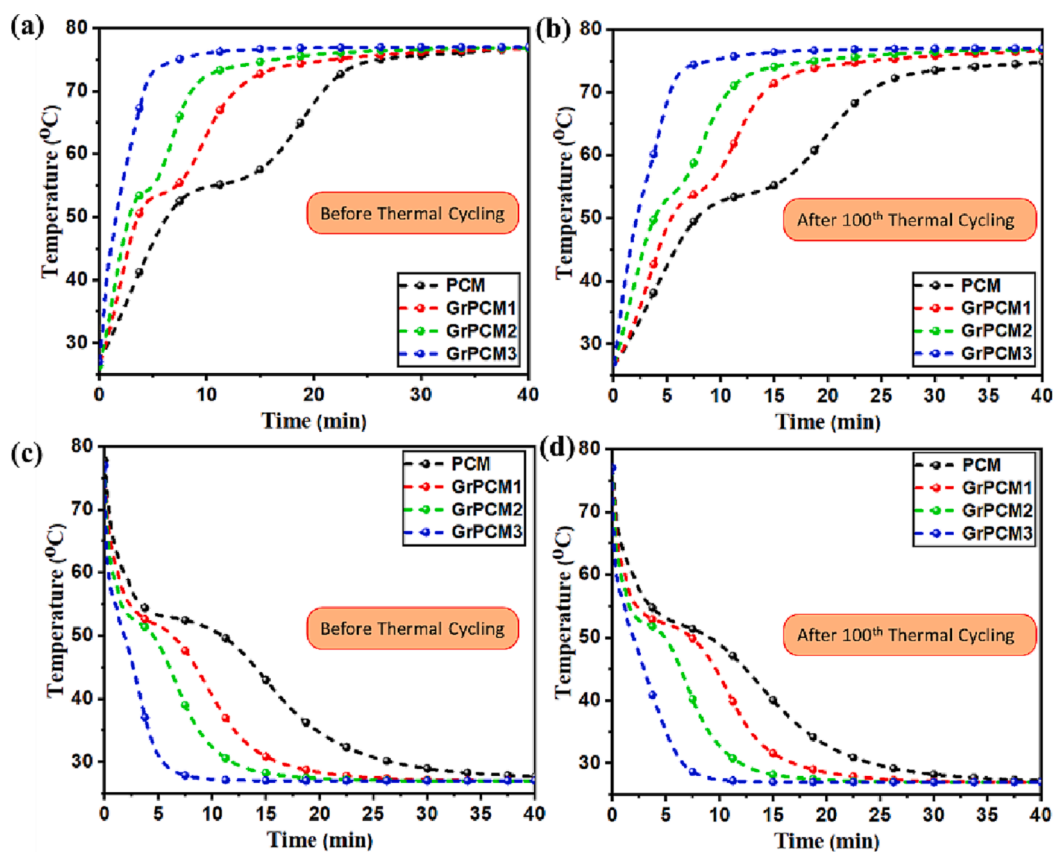

Fig. 10. *T*-history of various GrPCM nanocomposites under melting and solidification cycling: (a-b) heat storage and (c-d) heat release measurement.
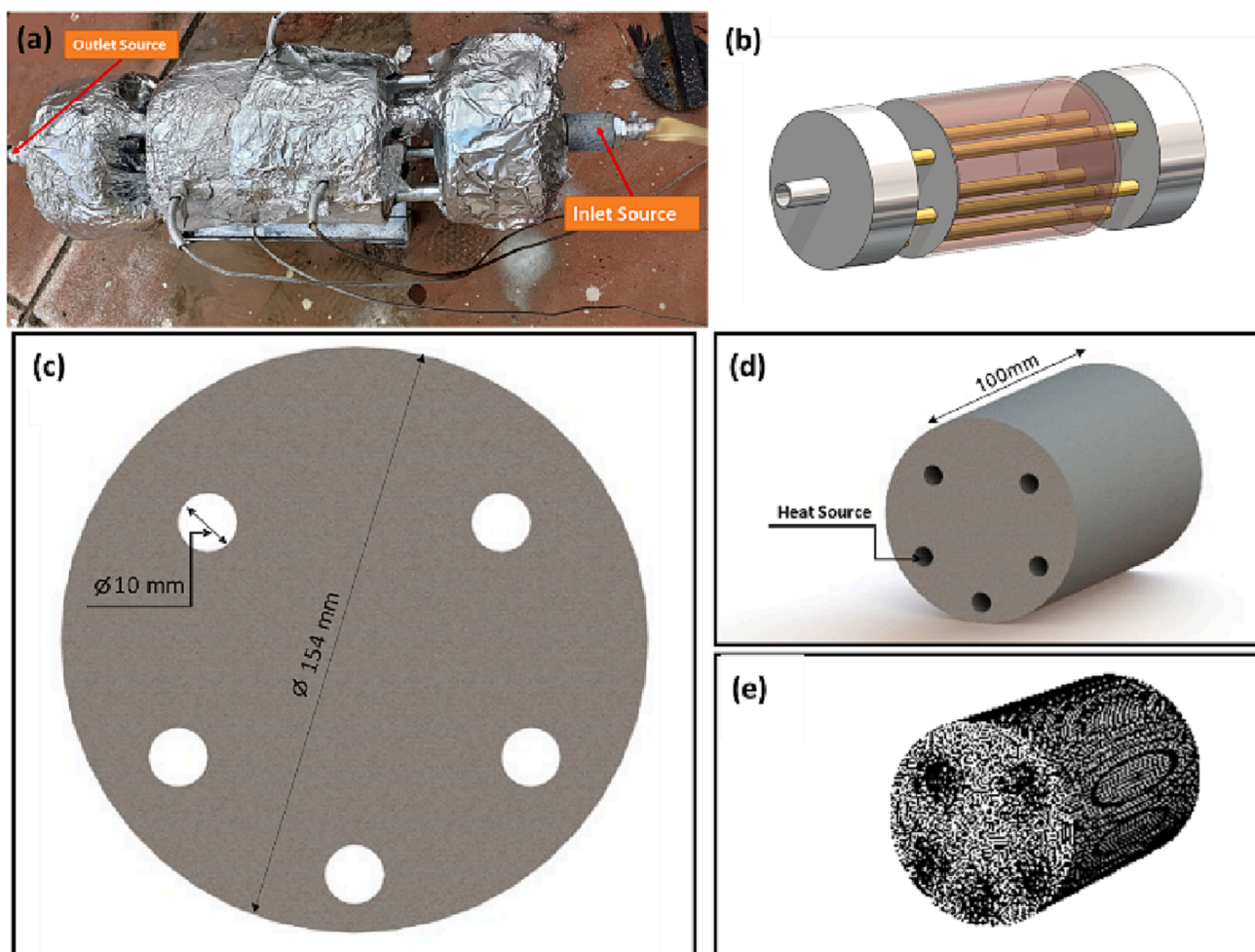
Fig. 11. (a) Experimental setup (b) manufacturing drawing of the cylindrical tank Schematic illustration (c-e) COMSOL simulated tank with dimensions [33].

shown in Fig. 9(a) and (b). The outcome suggests that increasing the graphene content in the nanocomposite increases the nanocomposite's overall thermal performance and conductivity. However, after 100 cycles of melting and solidifying, the conductivity of GrPCM nanocomposites decreases. After 100 cycles, the decrease in the thermal conductivity for 10 wt% and 15 wt% was observed to be lower as compared to 5 wt%. This can be explained by the nanocomposite's decreased stability caused by a higher carbon content after repeated thermal cycling. It was found that even after melting and solidification cycling for a long time, the thermal conductivities of the synthesized GrPCM nanocomposites were still significantly higher than PCM.

The PCM has a thermal conductivity of 0.26 W/m K, whereas GrPCM was found to have thermal conductivities of 4.43 W/m K, 7.92 W/m K, and 12.63 W/m K, respectively, for graphene contents of 5 %, 10 %, and 15 %, respectively. While the thermal conductivity of GrPCM nanocomposites after 100 thermal cycles were calculated to be 3.51 W/m K, 6.93 W/m K, and 11.09 W/m K indicating a decrease of 20.4 %, 12.27 %, and 11.91 % than the original thermal conductivity of nanocomposites. This suggests that the thermal melting/solidifying cycling has a detrimental effect on the nanocomposite's thermal conductivity, as shown in Fig. 7(a-b). The uneven distribution of PCM between the graphene nanosheets during melting and solidification cycling is the leading cause of the poor effect on thermal conductivity. The compatibility of PCM and graphene nanosheets after continuous thermal cycles, interfacial resistance, and the surface structure of the graphene nanosheets in the samples were found to be in good agreement with the results of earlier studies [43–46], thus indicating the GrPCM nanocomposite is a promising material for long-term operation. The thermal diffusivity was

determined on the basis of thermal conductivity findings for different GrPCM nanocomposites. Fig. 9(c) shows how the carbon content affects the thermal diffusivity of GrPCM nanocomposites. The obtained results showed that different GrPCM samples with various graphene contents had thermal diffusivity that was comparable to thermal conductivity. The following formula was used to calculate the thermal diffusivity enhancement in order to make it easier to understand:

$$\alpha_{enhancing} = \frac{\alpha_{GrPCM}}{\alpha_{PCM}} \tag{8}$$

where alpha is the thermal diffusivity of the nanocomposite and phase change material, respectively. The outcome showed that the nanocomposite's thermal diffusivity rose as graphene content rose. Compared to phase change material, this is primarily due to improved thermal conductivity and volume distribution (pore availability). The thermal diffusivity increases by a factor of 19.15 to 48.65 when there is a 15 wt% concentration of graphene present and then slightly decreases by a factor of 12.50 to 49.75 in the solid phases after 100 thermal cycles. In previous reports, various studies conducted on the enhancement of PCMs thermal conductivity are presented in Table 5 [43,46–50]. A wide range of PCM and various composites containing different graphene content, 1–20 wt%, were investigated. All the composites had an increase in thermal conductivity that ranged from 0.28 to 45. The change in measured thermal conductivity over a wide range can be attributed to different qualities of graphene materials, which were fabricated using other chemical methods or thermal treatments, and differences in the initial PCM material. The thermal conductivity results obtained were
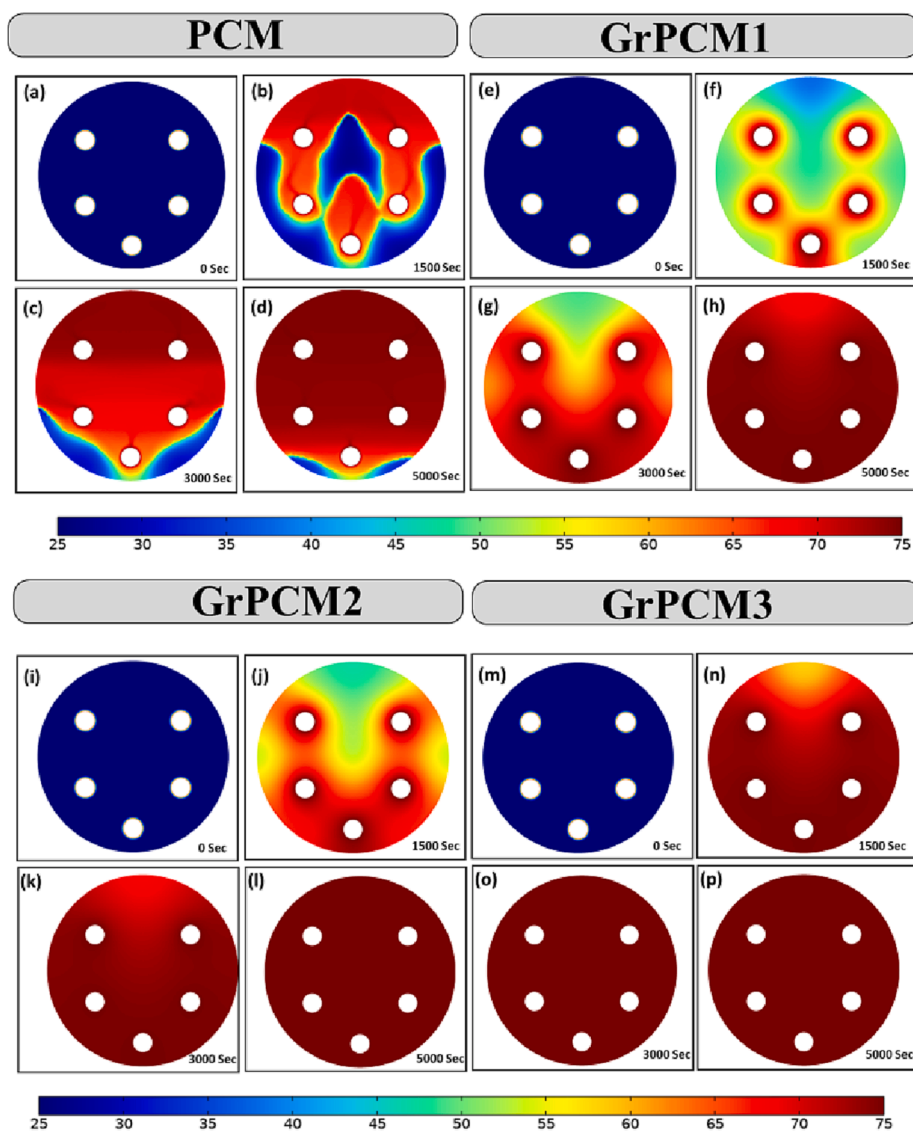
Fig. 12. COMSOL simulation during melting phase for (a-d) pure *n*-hexacosane, (e-h) GrPCM1, (i-l) GrPCM2 and (m-p) GrPCM3 in the thermal heat storage tank.

found to be in good agreement with the reported literature.

Thermal transfer measurement

The GrPCM nanocomposites were measured for thermal (heat) storage and release using the *T*-history setup, as shown in Figure S5 (please refer to supplementary information). The temperature–time curves of different GrPCM nanocomposites during the thermal storage and release processes are shown in Fig. 10 (a-d), and the specifics of the setup and operation have been discussed in Section 3.2.3. The thermal storage procedure can be broken down into various phases. The temperature of the nanocomposite samples increases linearly with time during the initial stage, which lasts from 27 °C to 53 °C, where there is no phase transition. When compared to other nanocomposites, the nanocomposite with the higher carbon (Gr) content experiences a shorter temperature rise. The second stage then takes place between 54 °C and 75 °C, where the materials (*n*-hexacosane) undergo a phase change. The nanocomposite is then filled with the melted phase change material, which causes the temperature of the nanocomposite to rise quickly. According to Fig. 10(a) and (b), the overall time needed for thermal storage in these tests during temperature increase is 25.38 min, 17.42 min, and 8.79 min, respectively (before thermal cycling), while

the thermal storage after 100 cycles was 28.32 min, 19.22 min, and 9.51 min, respectively, times which were 10.38 %, 9.36 %, and 7.57 % longer. Fig. 10(c) and (d) depict various phases of the heat release curves of GrPCM nanocomposites.

Similarly, the overall thermal release times for different GrPCM nanocomposites, i.e., 5 wt%, 10 wt%, and 15 wt%, before thermal cycling were 32.41 min, 26.13 min, and 11.37 min, respectively, while the overall thermal release times after 100 thermal cycles were 36.48 min, 28.18 min, and 12.34 min, which were 11.15 %, 7.27 %, and 5.56 % longer than the release time if original GrPCM nanocomposite. The thermal storage/release process over time is typically lengthened due to melting/solidifying cycles. The morphological changes in the nanocomposite material's graphene that resulted in the accumulation of nanosheets and decreased heat transfer can be due to this behavior.

Heat storage system

The as-prepared PCM impregnated graphene nanocomposite was investigated inside a thermal storage tank to understand the change in phases with respect to time during melting and cooling cycle as shown in Fig. 11 (a) [33]. The motive behind the study is to understand the heat transfer between fluid and nanocomposite having different carbon
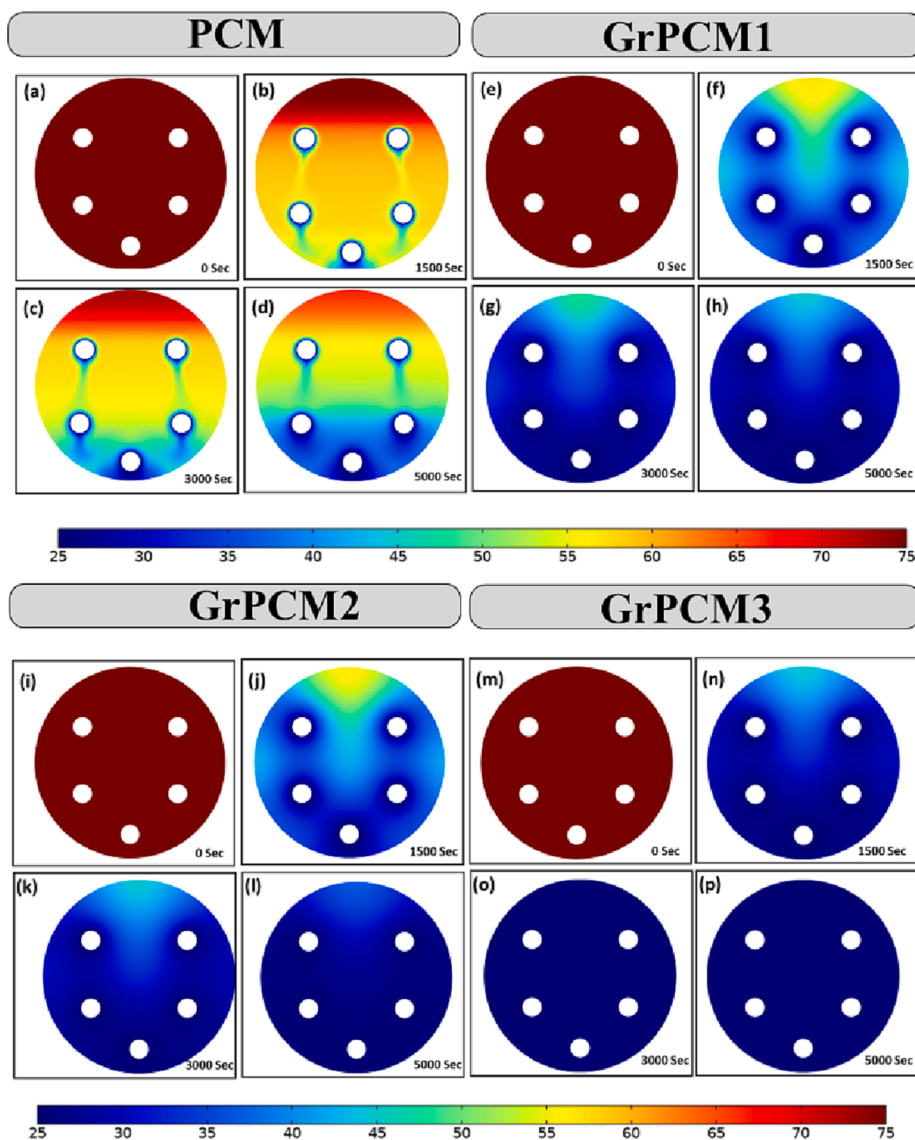
Fig. 13. COMSOL simulation of (a-l) pure *n*-hexacosane and (m-x) GrPCM3 in the storage tank.
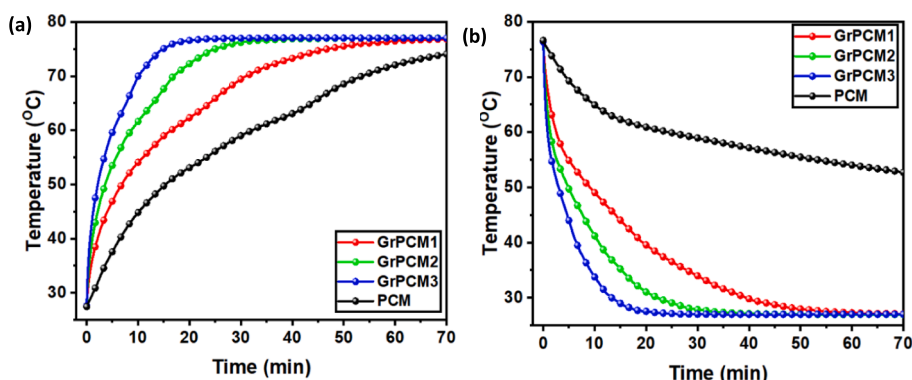

Fig. 14. Simulated Temperature vs Time graph for PCM nanocomposite in the thermal heat storage tank.

concentration. To begin with, a COMSOL simulation was performed of a cylindrical tank filled with different PCM material and a heat source as a fluid which is at 70 ℃ as shown in Fig. 11 (b-e) [33].

The COMSOL simulations of melting and solidification cycles were performed for pure PCM and GrPCM nanocomposites with respect to time as shown in Figs. 12 and 13. The figures from the simulations indicate that the GrPCM3 absorbs more energy efficiently as compared to other nanocomposites and pure phase change material. The complete melting of GrPCM1, GrPCM2, GrPCM3 was observed significantly earlier than pure PCM with reduction of 42.25 %, 68.15 %, and 80.25 %
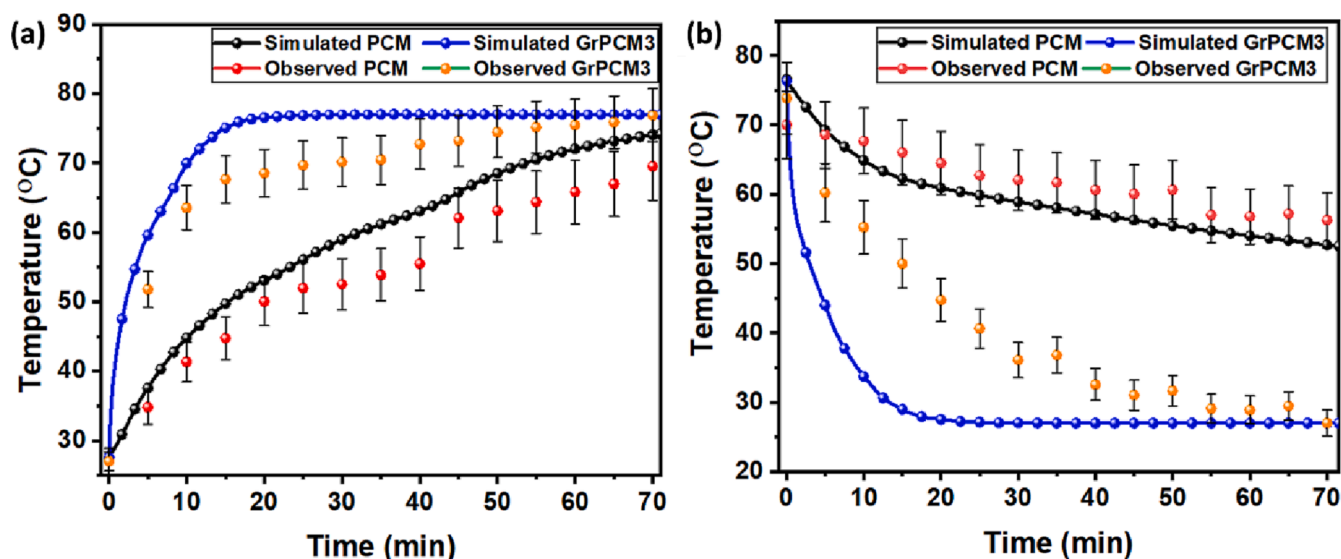
Fig. 15. (a) Melting, and (b) solidification thermal cycle performance of PCM and GrPCM3 composite in the heat storage tank.

in time during melting cycle as shown in Fig. 14(a). This substantial reduction in time during the melting cycle can be attributed to faster heat transfer from the source to the PCM due to the presence of highly conductive graphene, which holds the phase change material. Similarly, during solidification cycle, the inlet source fluid was kept at room temperature and circulated to absorb the energy from the PCM materials.

It was observed that the heat transfer between the source and GrPCM was efficient as compared to pure PCM taking 0.1, 0.05 and 0.03 less time for GrPCM1, GrPCM2, and GrPCM3 compared to PCM (70 min) as shown in Fig. 14 (b). The result confirms GrPCM3 can be an excellent composite material for efficient heat transfer processes. These are substantial reductions in time during the heat transfer process between the source and GrPCM nanocomposite and can serve as an efficient method to store and retrieve thermal energy for engineering applications.

To validate the observations from the COMSOL simulation, an experimental setup was designed consisting of a cylindrical tank with five tubes, for fluid circulation and temperature sensors, as shown in Fig. 11 (a). The water was used a circulating fluid throughout the experiment with 40 LPH flow rate at 70℃. The fabricated tank was designed in such a way that the water is evenly distributed among the five pipes in the cylindrical tank which eventually helps in better heat transfer, storage, and retrieval of energy in the GrPCM nanocomposite during the melting and solidification cycle.

Firstly, the GrPCM nanocomposite stores sensible heat due to the high-temperature difference between the solid GrPCM nanocomposite and inlet fluid. Once the temperature of GrPCM reaches close to its transition temperature, the composite begins to store latent heat, which is released much later, resulting in an efficient heat management system. Fig. 15 (a, b) shows the experimental results in accordance with the simulated observation which was found in good agreement. Thus, the as-synthesized nanocomposite can be used as a promising material for industrial applications.

Conclusion

The current work shows a scalable and versatile chemical method to fabricate *n*-hexacosane-impregnated graphene nanosheet composite as a promising phase change material (GrPCM) for energy storage systems. The method described is distinct from traditional preparation methods involving intricate synthesis mechanisms. The GrPCM nanocomposites (5 wt%, 10 wt%, and 15 wt%) were formed without any chemical reaction between the components, which was confirmed by structural and morphological studies. The graphene nanosheet serves as a supporting structure and prevents PCM from exuding. It also enhances the nanocomposites' thermal stability, diffusivity, and conductivity. The increase in thermal conductivity caused by the carbon content is confirmed by infrared imaging, which also develops a stable PCM nanocomposite. Since long-lasting cyclic performance is an essential factor for industrial applications, a thorough investigation was conducted to examine the changes in thermophysical properties of the as-synthesized nanocomposite after thermal cycling. In-depth research was done on several characteristics, such as latent heat, transition temperature, impregnation quantity, thermal conductivity, stability, and heat storage/release. Enhancing the thermal conductivity, stabilizing the nanocomposite, and addressing the exudation issue of PCMs during their liquid state are all achieved by adding graphene nanosheets to phase-change materials. Thus, the fabricated GrPCM can therefore serve as a tremendous energy storage material for industrial applications.

CRediT authorship contribution statement

Sakshum Khanna: Conceptualization, Investigation, Validation, Writing – original draft, Writing – review & editing. **Sagar Paneliya:** Investigation, Validation. **Parth Prajapati:** Writing – review & editing. **Rakesh Chaudhari:** Writing – review & editing. **Jay Vora:** Writing – review & editing. **Hussam Jouhara:** Writing – review & editing.

Declaration of Competing Interest

The authors declare that they have no known competing financial interests or personal relationships that could have appeared to influence the work reported in this paper.

Data availability

No data was used for the research described in the article.

Author Contribution

All authors have read and agreed to the published version of the manuscript.

Appendix A. Supplementary data

Supplementary data to this article can be found online at https://doi.org/10.1016/j.tsep.2023.101712.

References

[1] H. Jouhara, A. Żabnieńska-Góra, N. Khordehgah, D. Ahmad, T. Lipinski, Latent thermal energy storage technologies and applications: A review, Int. J. Thermofluids. 1 (5) (2020 Aug), 100039.

[2] S.E. Kalnas, B.P. Jelle, Phase change materials and products for building applications: A state-of-the-art review and future research opportunities, Energ. Buildings 94 (2015) 150–176.

[3] O. Okogeri, V.N. Stathopoulos, What about greener phase change materials? A review on biobased phase change materials for thermal energy storage applications, Int. J. Thermofluids. 1 (10) (2021 May), 100081.

[4] A. Amini, J. Miller, H. Jouhara, An investigation into the use of the heat pipe technology in thermal energy storage heat exchangers, Energy 1 (136) (2017 Oct) 163–172.

[5] R. Cao, H. Liu, S. Chen, D. Pei, J. Miao, X. Zhang, Fabrication and properties of graphene oxide-grafted-poly (hexadecyl acrylate) as a solid-solid phase change material, Compos. Sci. Technol. 149 (2017) 262–268.

[6] S. Paneliya, S. Khanna, P. Prajapati, A. Borad, Computational analysis of copper@ paraffin composite in a cylindrical cavity for enhanced thermal energy storage system, Mater. Today:. Proc. 43 (2021) 541–546.

[7] A.P. Singh, S. Khanna, S. Paneliya, H. Hinsu, Y. Patel, B. Mehta, Preparation and characterization of solid-state neopentyl glycol/expanded graphite micro composite for thermal energy storage applications, Materials Today: Proceedings (2020).

[8] J. Giro-Paloma, M. Martínez, L.F. Cabeza, A.I. Fernández, Types, methods, techniques, and applications for microencapsulated phase change materials (MPCM): A review, Renew. Sustain. Energy Rev. 53 (2016) 1059–1075.

[9] J.M. Jalil, S.M. Salih, Experimental and numerical investigation of paraffin wax as thermal insulator in a double glazed window, J. Storage Mater. 35 (2021), 102173.

[10] R. Li, Y. Zhou, X. Duan, Nanoparticle enhanced paraffin and tailing ceramic composite phase change material for thermal energy storage, Sustainable Energy Fuels 4 (9) (2020) 4547–4557.

[11] B. Kalidasan, A.K. Pandey, S. Shahabuddin, M. George, K. Sharma, M. Samykano, V.V. Tyagi, R. Saidur, Synthesis and characterization of conducting Polyaniline@ cobalt-Paraffin wax nanocomposite as nano-phase change material: Enhanced thermophysical properties, Renew. Energy 173 (2021) 1057–1069.

[12] Z. Zhang, Y. Liu, J. Wang, L. Sun, T. Xie, K. Yang, Z. Li, Preparation and characterization of high efficiency microencapsulated phase change material based on paraffin wax core and SiO2 shell derived from sodium silicate precursor, Colloids Surf A Physicochem Eng Asp 26 (2021), 126905.

[13] S. Paneliya, S. Khanna, A.P. Singh, Y.K. Patel, A. Vanpariya, N.H. Makani, R. Banerjee, I. Mukhopadhyay, Core shell paraffin/silica nanocomposite: A promising phase change material for thermal energy storage, Renew. Energy 167 (2021) 591–599.

[14] V. Guichet, B. Delpech, N. Khordehgah, H. Jouhara, Experimental and theoretical investigation of the influence of heat transfer rate on the thermal performance of a multi-channel flat heat pipe, Energy 1 (250) (2022 Jul), 123804.

[15] X. Zuo, X. Zhao, J. Li, Y. Hu, H. Yang, D. Chen, Enhanced thermal conductivity of form-stable composite phase-change materials with graphite hybridizing expanded perlite/paraffin, Sol. Energy 209 (2020) 85–95.

[16] H. Sivasankaran, K. Ishikawa, E. Einarsson, S. Aikawa, T. Inoue, P. Zhao, M. Watanabe, S. Chiashi, J. Shiomi, S. Maruyama, Temperature dependent thermal conductivity increase of aqueous nanofluid with single walled carbon nanotube inclusion, Mater. Express 2 (2012) 213–223.

[17] T. Xu, Q. Chen, G. Huang, Z. Zhang, X. Gao, S. Lu, Preparation and thermal energy storage properties of d-Mannitol/expanded graphite composite phase change material, Sol. Energy Mater. Sol. Cells 155 (2016) 141–146.

[18] Y. Cui, C. Liu, S. Hu, X. Yu, The experimental exploration of carbon nanofiber and carbon nanotube additives on thermal behavior of phase change materials, Sol. Energy Mater. Sol. Cells 95 (2011) 1208–1212.

[19] T.X. Li, J.H. Lee, R.Z. Wang, Y.T. Kang, Enhancement of heat transfer for thermal energy storage application using stearic acid nanocomposite with multi-walled carbon nanotubes, Energy 55 (2013) 752–761.

[20] A. Karaipekli, A. Sarı, K. Kaygusuz, Thermal conductivity improvement of stearic acid using expanded graphite and carbon fiber for energy storage applications, Renew. Energy 32 (13) (2007) 2201–2210.

[21] G. Fang, H. Li, Z. Chen, X. Liu, Preparation and characterization of stearic acid/ expanded graphite composites as thermal energy storage materials, Energy 35 (12) (2010) 4622–4626.

[22] H. Zhang, X. Gao, C. Chen, T. Xu, Y. Fang, Z. Zhang, A capric–palmitic–stearic acid ternary eutectic mixture/expanded graphite composite phase change material for thermal energy storage, Compos. A Appl. Sci. Manuf. 87 (2016) 138–145.

[23] X. Yang, Y. Yuan, N. Zhang, X. Cao, C. Liu, Preparation and properties of myristic–palmitic–stearic acid/expanded graphite composites as phase change materials for energy storage, Sol. Energy 99 (2014) 259–266.

[24] R. Wen, X. Zhang, Y. Huang, Z. Yin, Z. Huang, M. Fang, Y.g. Liu, X. Wu, Preparation and properties of fatty acid eutectics/expanded perlite and expanded vermiculite shape-stabilized materials for thermal energy storage in buildings, Energ. Buildings 139 (2017) 197–204.

[25] P. Hu, J.-J. Yu, X.-W. Wang, preparation and thermal performance of palmitic acid/expanded graphite composite phase change materials, J. Eng. Thermophysics 38 (2017) 464–469.

[26] D. Zhou, J. Yuan, Y. Zhou, Y. Liu, Preparation and characterization of myristic acid/expanded graphite composite phase change materials for thermal energy storage, Sci. Rep. 10 (1) (2020) 1–11.

[27] K. Golemanov, N.D. Denkov, S. Tcholakova, M. Vethamuthu, A. Lips, Surfactant mixtures for control of bubble surface mobility in foam studies, Langmuir 24 (2008) 9956–9961.

[28] L.-W. Fan, Z.-Q. Zhu, Y. Zeng, Q. Lu, Z.-T. Yu, Heat transfer during melting of graphene-based composite phase change materials heated from below, Int. J. Heat Mass Transf. 79 (2014) 94–104.

[29] Y.B. Tao, C.H. Lin, Y.L. He, Preparation and thermal properties characterization of carbonate salt/carbon nanomaterial composite phase change material, Energ. Conver. Manage. 97 (2015) 103–110.

[30] M. Amin, N. Putra, E. Kosasih E, E. Prawiro, R. Luanto R, T. Mahlia, Thermal properties of beeswax/graphene phase change material as energy storage for building applications. Appl. Therm. Eng. 5(2017) 273-80.

[31] S. Khanna, P. Marathey, A. Vanpariya, S. Paneliya, I. Mukhopadhyay, In-situ preparation of titania/graphene nanocomposite via a facile sol–gel strategy: A promising anodic material for Li-ion batteries, Mater. Lett. 300 (2021), 130143.

[32] S. Paneliya, S. Khanna, N.H. Makani, R. Banerjee, I. Mukhopadhyay, Highly stable n-hexacosane loaded exfoliated graphite nanosheets for enhanced thermal energy storage application, J. Storage Mater. (2022), 103903.

[33] S. Khanna, S. Paneliya, P. Prajapati, I. Mukhopadhyay, H. Jouhara, Ultra-stable silica/exfoliated graphite encapsulated n-hexacosane phase change nanocomposite: A promising material for thermal energy storage applications, Energy 123729 (2022).

[34] G. Wang, X. Shen, Wang, J. Yao, J. Park, Synthesis and characterisation of hydrophilic and organophilic graphene nanosheets. Carbon 5(2009) 1359-64.

[35] P. Tatsidjodoung, N. Le Pierrès, L. Luo, A review of potential materials for thermal energy storage in building applications, Renew. Sustain. Energy Rev. 18 (2013) 327–349.

[36] Y. Yuan, Y. Yuan, N. Zhang, Y. Du, X. Cao, Preparation and thermal characterization of capric–myristic–palmitic acid/expanded graphite composite as phase change material for energy storage, Mater. Lett. 125 (2014) 154–157.

[37] X. Wang, B. Li, Z. Qu, J. Zhang, Z. Jin, Effects of graphite microstructure evolution on the anisotropic thermal conductivity of expanded graphite/paraffin phase change materials and their thermal energy storage performance, Int. J. Heat Mass Transf. 1 (155) (2020 Jul), 119853.

[38] R. Wang, M. Han, Q. Zhao, Z. Ren, X. Guo, C. Xu, N. Hu, L. Lu, Hydrothermal synthesis of nanostructured graphene/polyaniline composites as high-capacitance electrode materials for supercapacitors, Scient. Rep. 7 (2017) 1–9.

[39] J. Sun, Z. Wu, Study on evaluation method of phase change material leaky degree for building, New Build. Mater. 7 (2004) 43–46.

[40] A. Sarı, A. Karaipekli, Preparation, thermal properties and thermal reliability of palmitic acid/expanded graphite composite as form-stable PCM for thermal energy storage, Sol. Energy Mater. Sol. Cells 93 (5) (2009) 571–576.

[41] H. Kao, M. Li, X. Lv, J. Tan, Preparation and thermal properties of expanded graphite/paraffin/organic montmorillonite composite phase change material, J. Therm. Anal. Calorim. 107 (1) (2012) 299–303.

[42] S. Khanna, P. Marathey, S. Paneliya, P. Vinchhi, R. Chaudhari, J. Vora, Fabrication of graphene/Titania nanograss composite on shape memory alloy as photoanodes for photoelectrochemical studies: Role of the graphene, Int. J. Hydrogen Energy (2022), https://doi.org/10.1016/j.ijhydene.2022.02.050.

[43] K. Kumar, K. Sharma, S. Verma, N. Upadhyay, Experimental investigation of graphene-paraffin wax nanocomposites for thermal energy storage, Mater. Today:. Proc. 18 (2019) 5158–5163.

[44] K. Kant, A. Shukla, A. Sharma, P.H. Biwole, Heat transfer study of phase change materials with graphene nano particle for thermal energy storage, Sol. Energy 146 (2017) 453–463.

[45] A.G. Olabi, H.M. Maghrabie, O.H. Adhari, E.T. Sayed, B.A. Yousef, T. Salamah, M. Kamil, M.A. Abdelkareem, Battery thermal management systems: recent progress and challenges, Int. J. Thermofl. (2022), 100171.

[46] M.A. Ali, R.F. Viegas, M.S. Kumar, R.K. Kannapiran, M. Feroskhan, Enhancement of heat transfer in paraffin wax PCM using nano graphene composite for industrial helmets, J. Storage Mater. 26 (2019), 100982.

[47] M. Amin, N. Putra, E.A. Kosasih, E. Prawiro, R.A. Luanto, T.M. Mahlia, Thermal properties of beeswax/graphene phase change material as energy storage for building applications, Appl. Therm. Eng. 112 (2017) 273–280.

[48] C. Li, B. Xie, J. Chen, Graphene-decorated silica stabilized stearic acid as a thermal energy storage material, RSC Adv. 48 (2017) 30142–30151.

[49] P. Goli, S. Legedza, A. Dhar, R. Salgado, J. Renteria, A.A. Balandin, Graphene-enhanced hybrid phase change materials for thermal management of Li-ion batteries, J. Power Sources 248 (2014) 37–43.

[50] M. Qian, Z. Li, L. Fan, H. Wang, J. Xu, W. Zhao, F. Huang, Ultra-light graphene tile-based phase-change material for efficient thermal and solar energy harvest, ACS Applied Energy Materials. 6 (2020) 5517–5522.

[51] W. Cui, X. Li, X. Li, T. Si, L. Lu, T. Ma, Q. Wang, Thermal performance of modified melamine foam/graphene/paraffin wax composite phase change materials for solar-thermal energy conversion and storage, J. Clean. Prod. 20 (2022), 133031.

[52] M. Joseph, V. Sajith, Graphene enhanced paraffin nanocomposite based hybrid cooling system for thermal management of electronics, Appl. Therm. Eng. 25 (2019), 114342.